IEEE Access
Multidisciplinary | Rapid Review | Open Access Journal

Received August 23, 2020, accepted August 28, 2020, date of publication September 1, 2020, date of current version September 11, 2020.

Digital Object Identifier 10.1109/ACCESS.2020.3020853

Design of a Low-Profile, Frequency-Reconfigurable, and High Gain Antenna Using a Varactor-Loaded AMC Ground

SHUHUI YANG[1], (Member, IEEE), YINCHAO CHEN[2], (Senior Member, IEEE), CHENYIN YU[1], YAJIE GONG[1], AND FANGLU TONG[1]

[1]Department of Communication Engineering, Communication University of China, Beijing 100024, China
[2]Department of Electrical Engineering, University of South Carolina, Columbia, SC 29208, USA

Corresponding author: Shuhui Yang (yangshuhui2016@sina.com)

ABSTRACT In this paper, a novel planar active artificial magnetic conductor (AAMC) frequency-reconfigurable antenna printed on an FR4 substrate is proposed. Its AAMC metal pattern in a unit cell consists of a compound-five-ring nesting (CFRN) structure. It is loaded with only one varactor diode connected to the ground plane by a metallic via. In comparison to the conventional single-circle-ring AMC, the dimension of the CFRN-AMC has been reduced by about 44% along with a lower reflection loss. The frequency-reconfigurable antenna is constructed by placing a triangle-shaped dipole antenna operating at 1.8 GHz over the proposed active CFRN-AMC ground plane consisted with 5 × 5 periodic unit cells. The prototype of the CFRN-AMC-backed antenna was fabricated and measured. The measured results agree well with the simulated data. It is found that by tuning the capacitance applied on the CFRN-AMC from 2.2 to 0.5 pF, the frequency band of the AMC-based antenna has been varied in the range of 1.51 through 2.12 GHz along with the highest radiation gain of 5.37 dBi at 1.74 GHz. This gain is about 3.16 dB higher than that of the antenna without using the AMC. In addition, the presented CFRN-AMC-based antenna remains a very low profile, since the separation distance between the antenna and the AMC plane is only 2 mm or 0.012λ, where the λ denotes the wavelength at 1.8 GHz in free space.

INDEX TERMS Reconfigurable antenna, active artificial magnetic conductor, compound-five-ring nesting structure, varactor diode, low-profile, gain enhancement.

I. INTRODUCTION

Recently, reconfigurable antennas are attracting more and more attentions because of their capability for acquiring satisfied selectivity in polarization, radiation pattern, gain, as well as operation frequency bandwidth [1]–[6]. Their tunable and steerable features make the reconfigurable antennas be suitable in wireless communication systems for multifunction applications. For instance, a multi-polarization antenna can increase the channel capacity, alleviate the channel fading, and improve the communication reliability [3]–[5]. The frequency-tunable antennas can be employed to realize the dynamic spectrum allocation and frequency hopping [6]–[8].

There are mainly three techniques used for realizing the reconfigurable antennas, including embedding tunable devices on an antenna radiation patch [9]–[13], adjusting substrate materials [8], [14], [15], and adopting the active metasurface reflectors [2], [6], [18], [22].

It is worth noting that the early reconfigurable antennas were often fabricated by utilizing the ferrite materials, barium strontium titanate, and the substrates with magnetic or electric tunability [2], [8], [14], [15]. The disadvantages of these structures are mainly complex fabrication process and high cost. In [9]–[13], the p-n diodes were employed on the radiation patches or feedlines to carry out reconfigurable antennas. By controlling the ON and OFF states of the p-n junction diodes, the working frequencies of these antennas can be easily changed. But this method can only marginally improve an antenna's gain [17]–[19]. In the recent years, simple sandwich type planar artificial magnetic conductor (AMC) structures, mainly consisting of periodic unit cells, have been widely investigated, because of their in-phase-reflection characteristics. They have been further developed to enhance effectively the loaded antenna radiation

The associate editor coordinating the review of this manuscript and approving it for publication was Abhishek K. Jha.

performance [1], [4], [16]–[30], [36], [37]. In [16], an AMC with periodically arranged square patches was adopted to broaden the bandwidth for a combined antenna with loop and monopole elements. In [17], a coplanar waveguide miniaturized wearable antenna with an AMC structure was presented with the frequency bands of 2.4 and 5.8 GHz for WLAN application, where an AMC structure was used to improve radiation performance in the two frequency bands. To increase triband antenna's gains, two kinds of AMC reflectors characterized with three zero-phases of the reflection coefficient were proposed in [19] and [20], where the triband AMCs help the antennas obtain the gain enhancement up to 6.44 dB [20]. Although the above-mentioned AMCs [16]–[20] improve the radiation performance for the single or multi-band antennas, they are not reconfigurable antennas due to their structural limitations. In principle, use of electronic devices, such as lumped capacitors or varactor diodes, in a unit cell design, can flexibly manipulate the working frequency and bandwidth of the AMC. These phenomena have motivated researchers focusing on the design of active AMCs (AAMCs) and their applications to reconfigurable antennas [1], [2], [6], [18], [21]–[23]. As shown in [1], two broadband AAMCs were presented for P and L bands with different polarizations. In [2], an S-band frequency tunable antenna was implemented by using a square patch AMC loaded with varactor diodes. Similarly, in [6], an AAMC structure with different polarizations and tunable reflection characteristics were introduced. By using this AAMC, a multi-functional reconfigurable antenna was designed. To realize a tunable circularly polarized (CP) antenna, a two-layer AAMC was placed underneath a coplanar waveguide (CPW) monopole, which made the antenna's frequency and polarization characteristics dynamically change in a frequency band [21].

For the reported AAMCs or the reconfigurable AMC-backed antennas, there are mainly three limitations needed to be further improved, namely, a big number of electronic elements (e.g. varactor diodes) used in an AMC unit cell, high profile of AAMC-loaded antennas, and low gains of reconfigurable antennas. For example, in [6], each unit cell in the proposed mushroom-shaped AAMC required four varactor diodes, and the fabricated antenna-backed AMC plane consisted of 6 × 6 units and 144 diodes. Furthermore, the AAMC plane exhibited in [1] was composed of 16 × 16 units, and each unit cell was mounted with four or eight capacitors. This means that the total number of loaded elements reaches 1024 or 2048. It is apparent that AAMC using many varactor diodes will not only increase the production cost, but also increase the design difficulty level for DC biased circuits [23]. It is a great challenge to design an AMC-based reconfigurable antenna with lower profile. In [22], the distance between the antenna and the AMC reflector was 5 mm with the antenna gain of 3.7 dBi. Recently, the separation distance has been reduced to about 4 mm and this AMC-backed antenna's gain has been improved to be 5.1 dBi as shown in [18]. In [2], the separation distance

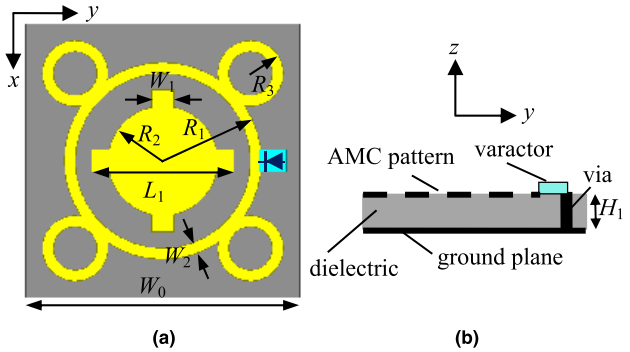

FIGURE 1. The geometry of the proposed active CFRN-AMC unit cell: (a) top view, and (b) side view. ($W_0 = 25$ mm, $W_1 = 2$ mm, $W_2 = 1$ mm, $L_1 = 13$ mm, $R_1 = 9$ mm, $R_2 = 5$ mm, $R_3 = 3$ mm).

was furtherly decreased to 3 mm, however, the AAMC-based antenna's gain remains about 5 dBi.

To address the above mentioned three limitations, in this paper, a novel low-profile, frequency-reconfigurable, and active AMC-backed antenna is proposed. The metal pattern of the AAMC's unit cell consists of a compound-five-ring and nesting (CFRN) structure which was evolved from the traditional AMC pattern with a single circle ring. In comparison to the single-circle-ring AMC, the size of the proposed CFRN-AMC has been reduced by about 44% along with a higher reflection amplitude, by using the same substrate and working at the same frequency. For the CFRN-AMC unit cell, there is only one varactor diode connected to the ground plane through a metallic via. The reduction of the number of varactor diodes will greatly improve the stability of the active AMC-backed antenna system and reduce the production cost. Furthermore, compared with the reported active AMC-backed antennas, the proposed CFRN-AAMC-based antenna system exhibits a high radiation gain of 5.37 dBi and has the lowest profile among the works published in [2], [6], [22], and [24]–[27]. Namely, the separation distance between the antenna and the AMC plane is only 2 mm, or 0.012λ at 1.8 GHz in free space.

II. DESIGN OF THE ACTIVE ARTIFICIAL MAGNETIC CONDUCTOR

Fig. 1 illustrates the proposed planar active AMC unit cell, which consists of a ground plane, a supporting substrate layer, and a metal layer with an AMC pattern. One reversely biased varactor diode is connected to the central metal ring and the ground through a metallic via.

As shown in Fig. 1(a), the AMC pattern is a compound-five-ring and nesting (CFRN) structure. The outer part is the compound-five-ring (CFR) structure, in which a big circle ring is tangent to four symmetrically arranged small circle rings. The inter part is formed by superposing a copper disc on a pair of the cross-shaped patches. The substrate layer is FR4 with the relative permittivity of 4.4 and the loss tangent of 0.02. The AMC pattern and the ground plane are both made of copper with the thickness of 0.035 mm. All the dimensions for the active AMC unit cell are provided in Fig. 1.

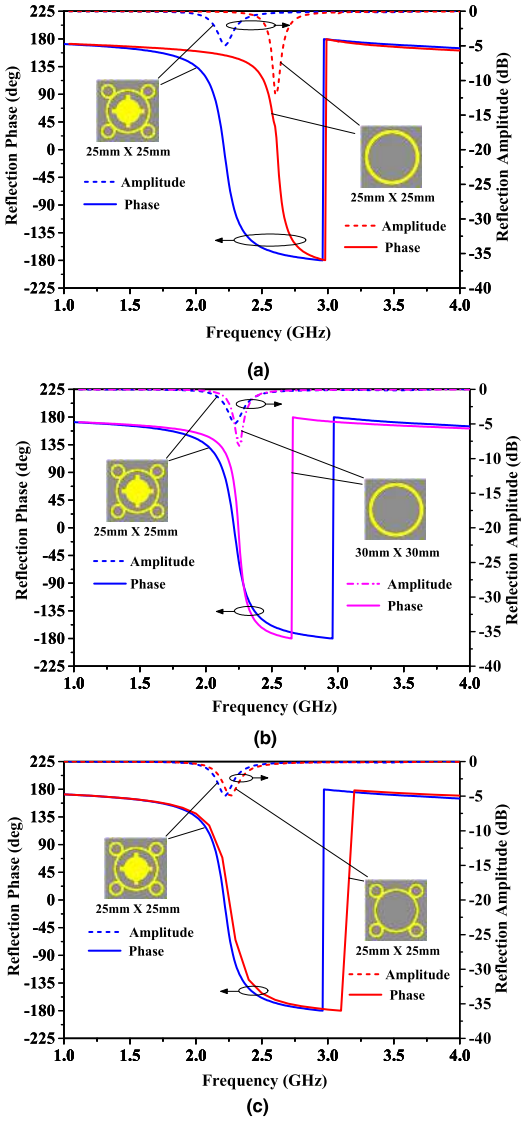

FIGURE 2. Comparison of the reflection properties of the AMCs realized by the CFRN structure and (a) single-circle-ring, (b) larger single-circle-ring, and (c) CFR.

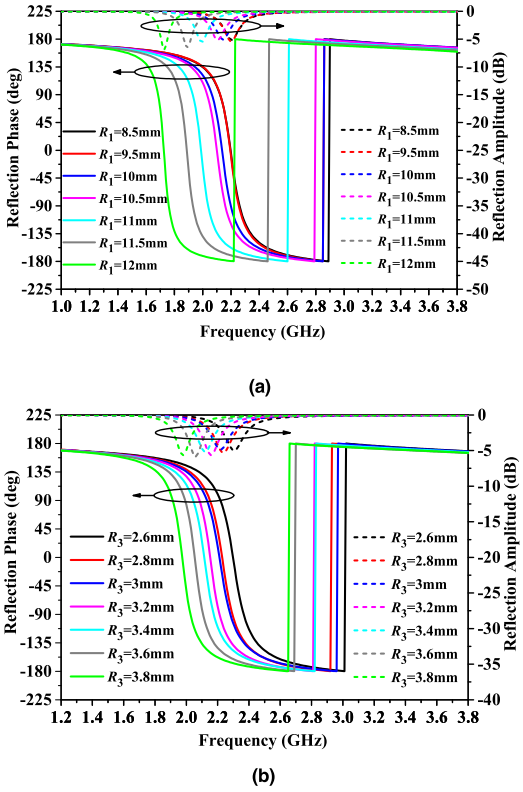

FIGURE 3. The reflection coefficients of the CFRN-AMC in the cases of (a) $R_1 = 8.5 \sim 12$ mm, and (b) $R_3 = 2.6 \sim 3.8$ mm.

Generally, the planar AMC's operation frequency is mainly determined by the size and shape of the AMC pattern as demonstrated in [1], [2], and [6]. It is very challenging to design a miniaturized AMC pattern while remaining the desired frequency band [13]–[15]. The presented CFRN-AMC was evolved from the one with the single-circle-ring. In comparison to a traditional single-band AMC using a circle or square ring, the CFRN-AMC exhibits not only the smaller size but also the lower reflection loss and wider frequency band.

Fig. 2(a) displays a comparison of the reflection characteristics of the AMCs realized by the CFRN structure and a circle ring pattern with same dimensions. It is observed that the zero-phase of the reflection coefficient for the CFRN-AMC occurs at 2.21 GHz along with the corresponding reflection amplitude of about –4.89 dB. Whereas the zero-phase for the single-circle-ring AMC is located at 2.65 GHz with the amplitude of –12.43 dB. Apparently, the proposed CFRN-AMC works at a lower frequency point with a higher reflection amplitude. By increasing the size of the unit cell, the single-circle-ring AMC's operation frequency band is decreased. As shown in Fig. 2(b), when the dimensions of the single-circle-ring AMC unit cell change from 25 mm × 25 mm to 30 mm × 30 mm, its zero-phase of the reflection coefficient has been shifted down to 2.22 GHz with the amplitude of –7.82 dB. This means that to achieve the similar working frequency, the area of the single-circle-ring AMC unit increases by additional 44% in comparison to that of the CFRN-AMC unit. Its reflection amplitude now moves to a high level along with the shifted frequency bandwidth. Fig. 2(c) shows the reflection properties for the CFRN-AMC with and without the inner disc and cross-shaped patch. It is found that the inner part of the AMC pattern does not increase the reflection amplitude but slightly reduce the zero-phase frequency.

Next, the influence of the dimensions of the CFRN structure on the AMC's reflection characteristics is studied. It is found that the reflection performance of AMC is sensitive to the outer part of the CFRN structure as depicted in Figs. 3(a) and 3(b). When varying the radii of the big circle ring, R_1, and the small circle rings, R_3, the frequency band of the AMC changes dramatically. If the values of R_1 are set as 12, 11, and 8.5 mm, and other parameters maintain as listed in Fig. 1, the zero-phases of the reflection coefficient will occur

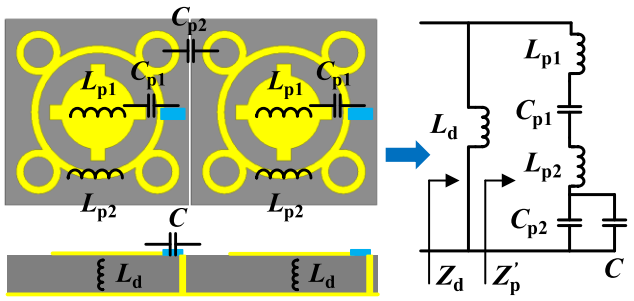

FIGURE 4. Equivalent circuit for the active CFRN-AMC.

at 1.76, 2.01, and 2.23 GHz, respectively. Similarly, when R_3 changes from 2.6 to 3.8 mm with the increase step of 0.2 mm, the operation frequency of the AMC will decrease gradually from 2.38 to 2.02 GHz.

To realize the frequency reconfigurable AMC with a compact geometry, as shown in Fig. 1, a reversely biased varactor is placed on the CFRN-AMC metal plane, which is connected to the ground by a metallic via. According to [1] and [4], the equivalent circuit for the unit cells of the active CFRN-AMCs is developed and illustrated in Fig. 4.

Herein, L_{p1} and L_{p2} denote the patch inductances existed in the inner and outer parts of the CFRN. C_{p1} and C_{p2} indicate the gap capacitance and the edge capacitance located in the gap between inner and outer parts of CFRN and the adjacent unit cells of the AMC. L_d represents the grounded dielectric slab inductance [1], [4], and C is the capacitance of the varactor diode. It is observed that the unit cell of the active CFRN-AMC can be characterized by a typical inductor-capacitor resonator. In order to help figure out the impact of C in the equivalent circuit, firstly, the passive CFRN-AMC without varactor diode is studied. To analyze its resonant frequency, the total surface impedance of the passive CFRN-AMC can be calculated as [1], [4],

$$Z(\omega) = Z_d // Z_p = j\omega L_d \frac{1-\omega^2 L_p C_p}{1-\omega^2 (L_d + L_p) C_p} \tag{1}$$

where Z_d and Z_p are the equivalent impedance of the grounded dielectric slab and patch impedance of the AMC pattern. L_p and C_p represent the series inductance and capacitance in Fig. 4 and are expressed by $L_p = L_{p1} + L_{p2}$ and $C_p = \frac{C_{p1} \cdot C_{p2}}{C_{p1} + C_{p2}}$.

Consequently, through enforcing the denominator of equation (1) equals to zero, the resonant frequency of the passive CFRN-AMC can be deduced as [6]

$$f_{r,passiveAMC} = \frac{1}{2\pi \sqrt{(L_d + L_p) C_p}}. \tag{2}$$

As seen from (2), the AMC's resonant frequency is highly dependent on L_d, L_p, and C_p, which are mainly determined by the AMC's physical structure. Namely, these distribution elements can be estimated by the following formulas [31]–[33]:

$$L_p = \mu_0 h \frac{l_{eff}}{w} \tag{3}$$

$$C_p = \varepsilon_0 \varepsilon_r \frac{S}{h} \tag{4}$$

$$L_d = \mu_0 \frac{\tan(k\sqrt{\varepsilon_r} h)}{k\sqrt{\varepsilon_r}} \tag{5}$$

where, μ_0 and ε_0 are the permeability and permittivity of free space, ε_r is the relative dielectric permittivity of the substrate, k represents the wavenumber, h is the thickness of the substrate, and s, l_{eff}, and w denote the area, efficient length and width of the microstrip line.

Since it is difficult to obtain a variable inductor in an integrated package in a series or parallel circuit for an equivalent AMC circuitry, a varactor diode is frequently used to adjust the total capacitance represented in formula (2).

In general, for the same varactor, a parallel-loaded AMC can work at a lower frequency, which reduces the size of an AMC [1], [13]. In this paper, the parallel loaded varactors are employed to realize the active CFRN-AMC. In comparison to the recently reported parallel-loaded AMCs [1], [6], the proposed active CFRN-AMC only requires one varactor diode in a unit cell rather than four in [6] or eight in [1]. The primary reason for this is that the AMC pattern utilized in [1] and [6] is simply a square patch or square ring. These patterns result in large coupling inductance and capacitance between the adjacent AMC unit cells. Thus, more varactor diodes are required to compensate the overall capacitance of the circuits. The proposed active CFRN-AMC brings about much less inductance and adjacent coupling capacitance between the unit cells through the small circle ring in the outer part of CFRN structure, so that only one varactor diode is needed to adjust the overall capacitance effectively. It is noticed that the reduction of the number of varactor diodes can not only cut down the cost efficiently and avoid the asymmetry of AMC structure caused by the difference of diodes, but also improve the stability of the active AMC performance.

Then, for the active CFRN-AMC, based on equations (1) and (2), its resonant frequency can be given as

$$f_{r,activeAMC} = \frac{1}{2\pi \sqrt{(L_d + L_p) C_p'}} \tag{6}$$

where, $C_p' = \frac{C_{p1} \cdot C_{p2}'}{C_{p1} + C_{p2}'}$ and $C_{p2}' = C_{p2} + C$. Considering that $C_p' > C_p$, comparison of equations (2) and (6) leads to

$$f_{r,passiveAMC} > f_{r,activeAMC} \tag{7}$$

which, apparently, indicates that the varactor capacitance allows not only steering the operation band for the AMC but also lowering its resonant frequency for reducing the AMC's dimension.

Fig. 5 displays the active CFRN-AMC's reflection performance in the cases for different capacitance values of the varactor diode. In Fig. 5(a), it is observed that with the addition of the capacitance the AMC's operation frequency is steerable from 2.19 (with C = 0.1 pF) to 2.03 GHz (with C = 0.5 pF). When the capacitance varies from 0.6 to 3 pF with the increase step of 0.3 pF, the resonant frequency of the

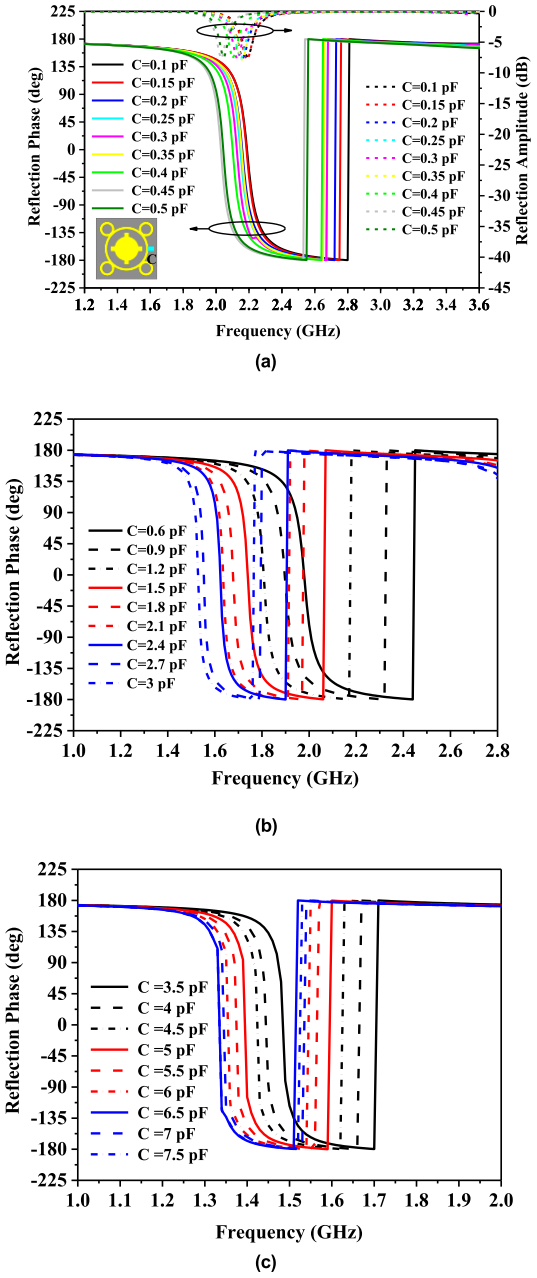

FIGURE 5. The phases of the reflection coefficients for the active CFRN-AMC with the capacitance in the cases of (a) 0.1∼0.5 pF, (b) 0.6∼3 pF, and (C) 3.5∼7.5 pF.

AMC gradually changes from 1.98 to 1.46 GHz as depicted in Fig. 5(b). Note that, as C equals to 1.2 pF, the zero-phase of the reflection coefficient has shifted from 2.21 GHz for no varactor diode as shown in Fig. 2(a) to the aimed frequency of 1.81 GHz. This phenomenon further indicates that the varactor is very positive to lower the working frequency and to minimize the size of the CFRN-AMC. In Fig. 5(c), along with C's change from 3.5 to 7.5 pF, the AMC's zero-phase of the reflection coefficient has altered from 1.51 to 1.32 GHz. When the capacitance of the varactor continues to increase, the AMC's operating frequency keeps on moving to a lower frequency in the band.

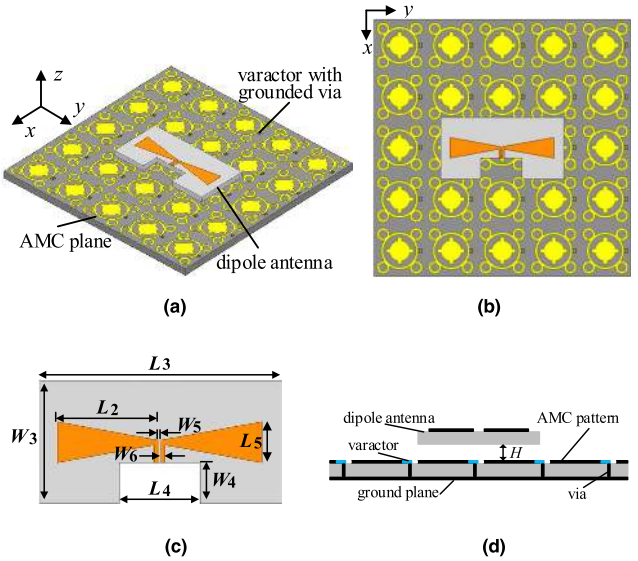

FIGURE 6. The configuration of the proposed active CFRN-AMC-based antenna: (a) 3D view, (b) top view, (c) the dipole antenna without AMC, and (d) side view ($L_2 = 25.6$ mm, $L_3 = 60$ mm, $L_4 = 20$ mm, $L_5 = 10$ mm, $W_3 = 30$ mm, $W_4 = 10$ mm, $W_5 = 0.6$ mm, and $W_6 = 1$ mm).

III. AMC-GROUNDED FREQUENCY-RECONFIGURABALE DIPOLE ANTENNA

A frequency-reconfigurable antenna system was designed to further verify the effectiveness of the proposed active CFRN-AMC structure. The antenna system consists of a dipole antenna and an electromagnetic-wave reflector formed by a 5 × 5 active CFRN-AMC array as shown in Fig. 6. A single-band triangle-shaped or bow-tie dipole antenna operated at 1.8 GHz was designed and printed on an FR4 substrate with the thickness of 1.6 mm. The bow-tie dipole antenna is fed by a pair of 50-Ω parallel strips (see Fig. 6(c)) which can be regarded as a parallel strip line balun [35] and is connected to the SMA connector. The bow-tie radiator and its feedline structure were produced by using a 0.035 mm-thick copper. To facilitate the welding test terminal, to shorten the feedline and to decrease antenna size, a rectangular-shaped groove is etched on the substrate. The dipole antenna is placed above the center of the AMC plane with the separation distance of H.

Fig. 7(a) shows the magnitude of S_{11} of the dipole antenna without the AMC, and it is seen that the antenna resonates at 1.8 GHz with the return loss of –15.8 dB. Figs. 7(b)-(d) display the magnitudes of S_{11} for the AMC-based antenna (ABA) with the diverse heights of H along with the different capacitances of the varactor diode loaded to the CFRN-AMC plane. It is observed that the ABA works well when H varies in a large range of variation. Especially, as shown in Fig. 7(b), even when H equals to 0.8 mm, the AMC-based antenna can still operate satisfactorily for this ultra-thin profile. It is also found that, for the different values of H, the varactor diodes can effectively adjust the ABA's working frequency bands.

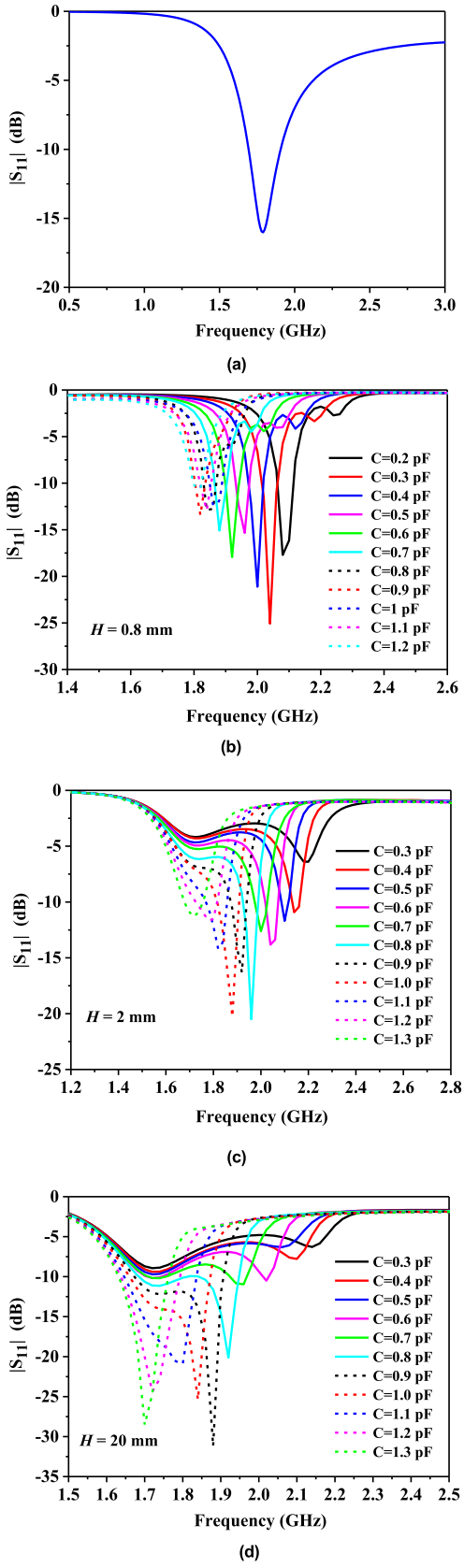

FIGURE 7. The magnitudes of S_{11} in dB for the dipole antennas: (a) without AMC, and using the CFRN-AMC plane with H being (b) 0.8 mm, (c) 2 mm, and (d) 20 mm.

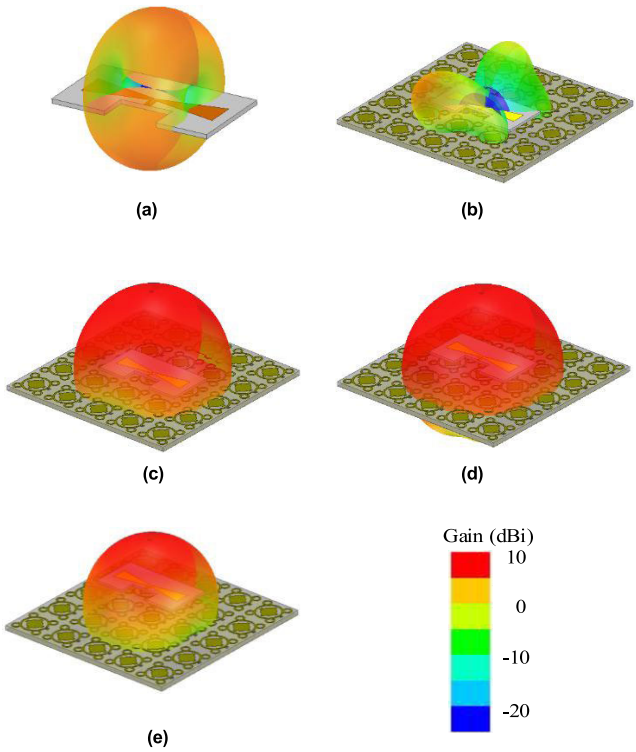

FIGURE 8. The 3D radiation patterns for the dipole antennas: (a) without AMC, and using the CFRN-AMC plane with H being (b) 0.8 mm, (c) 2 mm, (d) 10 mm, and (e) 20 mm.

In Fig. 7(b), when the capacitance C increases from 0.2 to 1.2 pF, the zero-phase of the reflection coefficient for the AMC plane varies correspondingly as demonstrated in Fig. 5. Affected by the working frequency band of the AMC reflection coefficient, the ABA's center frequency changes from 2.07 to 1.82 GHz. During the whole frequency scanning process, the return loss of the antenna maintains less than –10 dB and reaches the minimum value of –25.2 dB as C is 0.3 pF. Meanwhile, the bandwidth of the antenna almost remains unchanged with C being less than 0.7 pF. If H continues to increase, the ABA's operation band will slightly shift to the lower frequency due to the effect of the AMC. As shown in Fig. 7(c), for $H = 2$ mm, the ABA's working frequency has been tuned from 2.16 to 1.72 GHz when C varies from 0.4 to 1.3 pF.

When $H = 20$ mm, with the use of AMC reflector, the resonating frequency of the AMC-based antenna continues to move to the lower band from 2.02 to 1.68 GHz with C being increased from 0.6 to 1.3 pF.

Furtherly, Fig. 8 displays the 3D radiation patterns for the dipole antennas with and without the AMC reflector. The zero-phase of the reflection coefficient occurs at about 1.8 GHz along with the lumped capacitance of 1.2 pF. It is obvious that, as seen in Fig. 8(a), the single dipole antenna exhibits a typical omnidirectional doughnut-shaped radiation pattern with the maximum gain of 2.3 dBi.

As the dipole antenna is placed over the AMC plane, its radiation characteristics has been changed greatly. When H

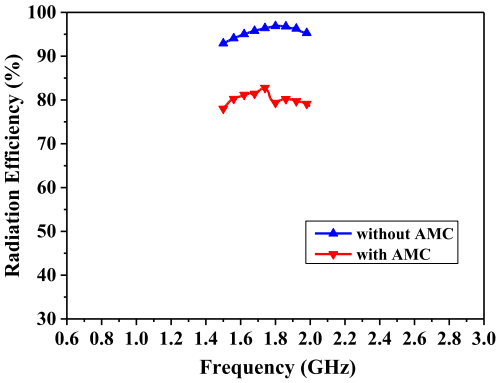

FIGURE 9. The radiation efficiencies for the dipole antennas with and without active AMC plane (H = 2 mm, C=1.2 pF).

is less than 2 mm, the return loss of the antenna remains less than –10 dB, and the radiation energy spreads out in the space above the ground plane. This leads to a low radiation gain. For example, when H is 0.8 mm, the AMC-based antenna's maximum gain becomes 0.4 dBi with the radiation pattern as shown in Fig. 8(b). When H is set as 2 mm, as depicted in Fig. 8(c), the radiation energy of the antenna is concentrated in the vertical direction above the AMC plane with a high gain of 5.5 dBi. It is more than twice of the maximum gain for the single dipole antenna without AMC.

With the increasement of H, the gain of the AMC-based antenna is further improved. Figs. 8(d)-(e) display the radiation patterns with H to be 10 and 20 mm, respectively, where a single main beam is directed in the direction right above the AMC plane while maintaining the nearly hemispherical radiation pattern. Correspondingly, the maximum gain of the AMC-based antenna has achieved at 6.2 and 6.4 dBi for the cases of H being 10 and 20 mm, respectively. Further simulation indicates that the proposed AMC-backed antenna reaches the maximum gain of 6.8 dBi when H is 25 mm (0.15λ). Herein, λ is the wavelength in free space at 1.8 GHz. If H is more than 25 mm, the gain will decrease.

Fig. 9 depicts the radiation efficiencies for the dipole antennas with and without AMC plane. It is found that the single dipole shows the typical high radiation efficiency (RE), indicating that it has good impedance matching and the dielectric loss around it is very small. The maximum RE achieves about 97% at 1.8 GHz. As expected, for the AMC-backed antenna, its RE decreases. This phenomenon is mainly attributed to the impedance mismatch and dielectric loss produced by the adjacent AAMC plane with lumped electronic elements. The AMC-backed antenna's RE reaches the maximum value of about 83% at 1.74 GHz. In fact, for a typical dipole antenna, its gain (G), directivity (D) and radiation efficiency (e_r) are related as follows:

$$G = D \cdot e_r \tag{8}$$

It can be seen that although AMC-backed antenna's radiation efficiency is reduced, its gain is higher than that of the single antenna due to the significant increasement of the directivity as displayed in Fig. 8.

TABLE 1. Comparisons between the dipole antennas with the proposed AMC and with PEC reflectors for different values of H.

Separation distance between antenna and reflector (H, mm)	Antenna with AMC reflector		Antenna with PEC reflector	
	$\|S_{11}\|$ (dB)	Maximum gain (dBi)	$\|S_{11}\|$ (dB)	Maximum gain (dBi)
2	–12.5	5.5	–0.5	–
5	–13.3	5.8	–1.2	–
10	–14.8	6.2	–2.1	–
20	–21.7	6.4	–5.8	–
25 (0.15λ)	–33.0	6.8	–8.5	–
30	–25.4	6.6	–12.6	6.8
42 (0.25λ)	–15.7	5.2	–26.8	7.2
55	–17.6	3.5	–19.6	5.7

* λ is the wavelength in free space at 1.8 GHz.

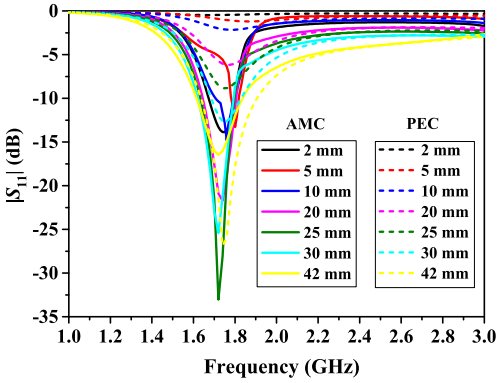

FIGURE 10. The magnitudes of S_{11} in dB for the dipole antennas with AMC and PEC reflectors for H changing from 2 to 42 mm.

A comparison study for different values of H for two cases of the antenna backed with a perfect electric conductor (PEC) reflector and with the AMC ground is performed as shown in Fig. 10 and Table 1.

It is apparently seen that, when H is less than or equals to 25 mm, for the case with the PEC reflector, the reflection coefficients of the antenna are all greater than –10 dB. Especially, when H is less than 10 mm, $|S_{11}|$ of the PEC-backed antenna is greater than –2.1 dB. These phenomena clearly indicate that the PEC-backed antenna system cannot work well with a low profile structure. When H is set as 42 mm or the quarter-wavelength in free space at 1.8 GHz, the PEC-backed antenna reaches the maximum gain of 7.2 dBi. Although the maximum gain of the AMC-backed antenna (H = 25 mm) is less than that of PEC-based antenna (H = 42 mm), it exhibits the important feature of low profile. It is also seen that, for H changing from 2 to 55 mm, the proposed AMC-backed antenna operates well with relatively high gains. By balancing the antenna's gain and its profile, the optimum value of H for the proposed AMC-backed antenna is selected as 2 mm, or 0.012λ at 1.8 GHz in free space.

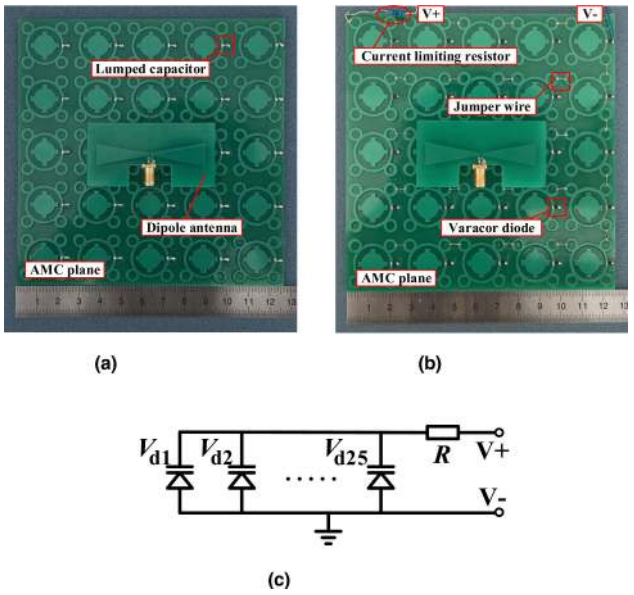

FIGURE 11. The photographs of the proposed CFRN-AMC antennas loaded with (a) lumped capacitors, (b) varactor diodes, and (c) the biasing circuit diagram of varactor diodes.

IV. EXPERIMENT ANALYSIS FOR THE AMC-BASED ANTENNA

The proposed active CFRN-AMC and AMC-based antenna were fabricated by employing a standard PCB process. The dipole antenna is placed in parallel to the AMC reflector through a foam layer. Fig. 11 displays the prototypes for the dipole antennas backed with two kinds of 5 × 5 array CFRN-AMC planes. One is mounted with the lumped capacitors and the other is with the varactor diodes. Each AMC plane was soldered with 25 chip capacitors or varactor diodes on the surface of the CFRN-AMC plane. The chip capacitors with the capacitance values of 0.3, 0.5, 1.0, 1.2, 1.5, 2.2, and 3.9 pF were used to form seven AMC planes, as shown in Fig. 11(a). SMV1231 with the SC-79 surface mount package was employed as the varactor diode in this design, whose typical capacitance values ranging from 0.487 to 2.350 pF, corresponding to the decrement of its reversed bias voltage from 12 to 0 V as seen in Fig. 11(b).

The measured magnitudes of S_{11} for the dipole antennas without and with the AMC using different lumped capacitors are plotted in Figs. 12(a) and 12(b). They agree well with the simulated ones. The small deviation is observed in Fig. 12(a) primarily due to the test interface conversion, welding technique and the fabrication tolerance. In addition to these reasons, the deviations in Fig. 12(b) may also come from the actual J-class chip packaging capacitor [6], whose standard capacity error is +/–5%. For $H = 2$ mm, when C is 2.2 pF, the measured center frequency of the AMC-based antenna is 1.51 GHz with $|S_{11}|$ of –14.8 dB. As C has been changed to 0.5 pF, the measured operation frequency of the AMC-based antenna has shifted to 2.12 GHz with the magnitude of S_{11} to be –12.3 dB.

Note that it may be relatively easy to design a passive wideband AMC reflector whose phase section spanning from

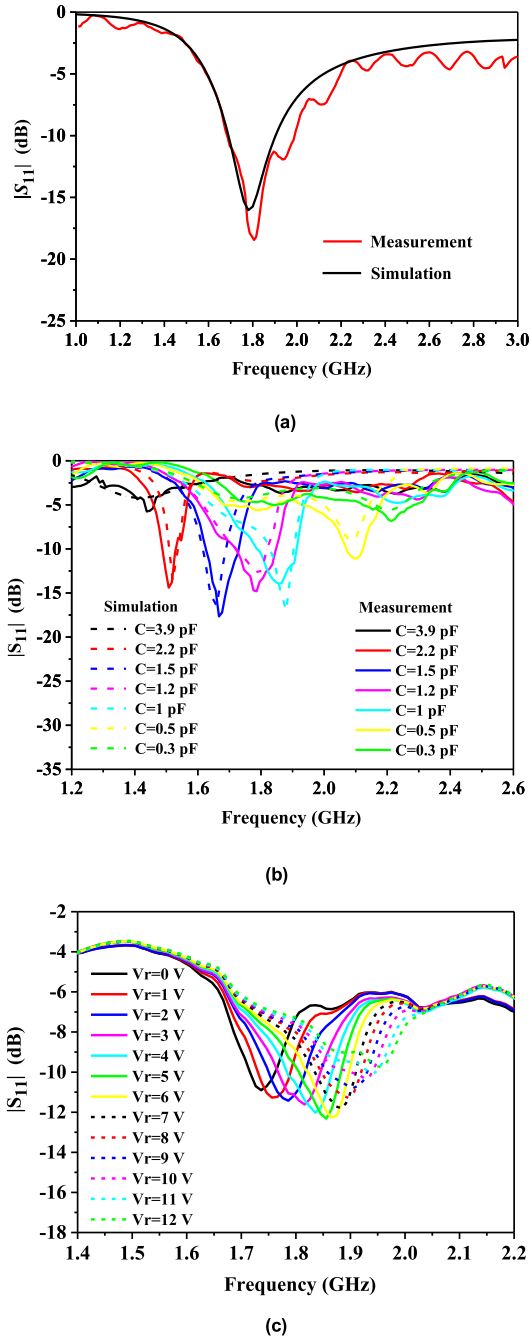

FIGURE 12. The measured magnitudes of S_{11} for the dipole antennas: (a) without AMC, and using CFRN-AMC with (b) lumped capacitors, and (c) varactor diodes.

+90° to –90° of the reflection coefficient (RC) can cover the frequency band of 1.51-2.12 GHz. However, the frequency of zero-phase of the RC for this kind of AMC is fixed and untunable. One of the key techniques to realize a frequency-tunable AMC-backed antenna is to fabricate an appropriate AAMC reflector with frequency reconfigurable characteristic by using electronic devices (e.g. lumped capacitors [1], varactor diodes [1], [2], [6], and capacitors with resistors [22]).

In Fig. 11(b), the jumper wires as the DC biasing lines connect the outer ring structures of all AMC units in series,

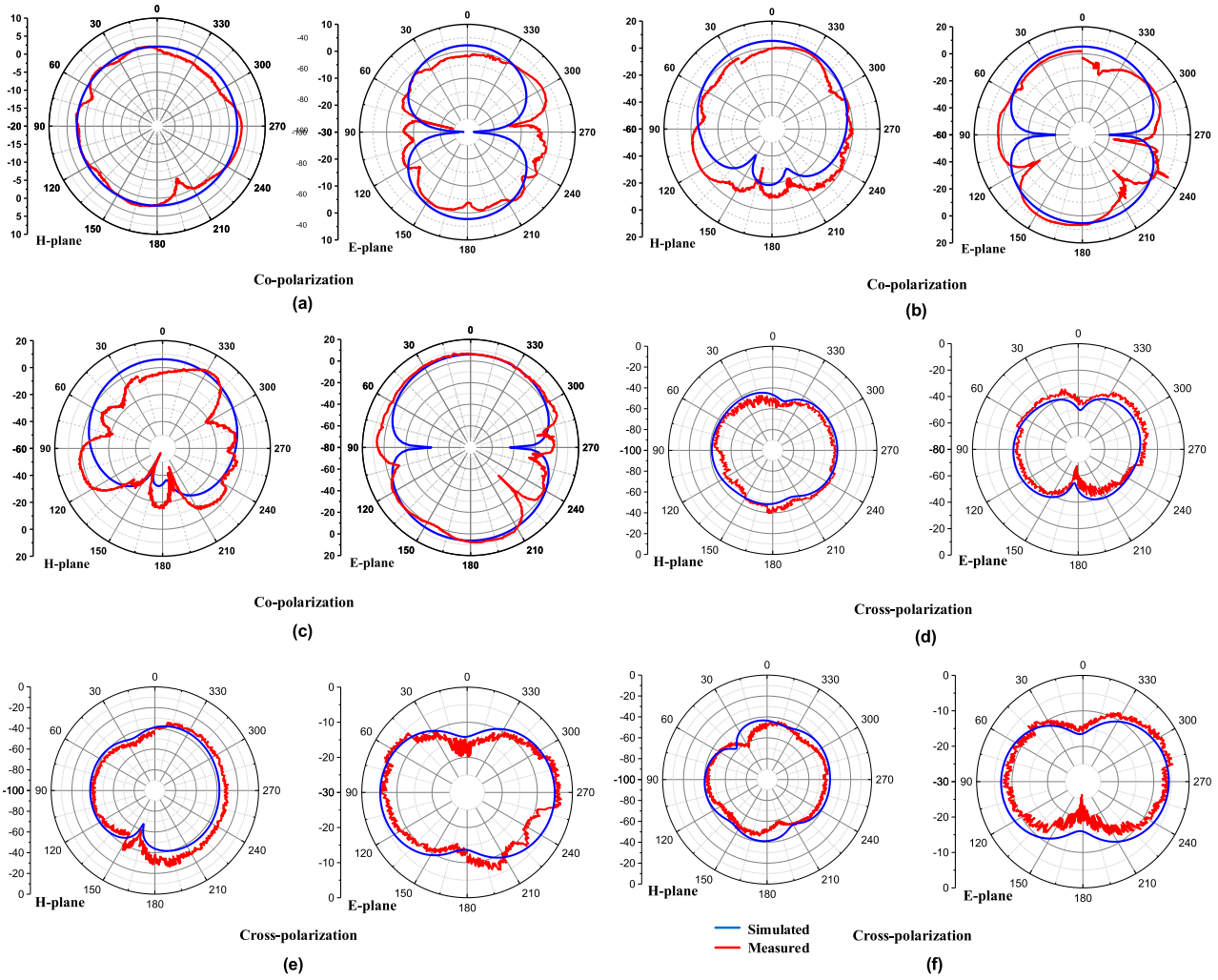

FIGURE 13. The measured and simulated radiation patterns for co-polarization of the antennas: (a) without AMC, and using AMC with *H* equals to (b) 2 mm, and (c) 10 mm, as well as the radiation patterns for cross-polarization of the antennas: (d) without AMC, and using AMC with *H* equals to (e) 2 mm, and (f) 10 mm.

and are linked to the positive port of the DC power supply denoted by V+, which provides the reversely biased voltage on the varactor diodes. To limit the biasing current, a lumped resistor of 10 kΩ is connected in series. Through metallic vias, the other ends of the varactor diodes are all connected to the ground plane of the AMC which is linked to the ground port of the DC source (V–). The biasing circuit diagram of varactor diodes is illustrated in Fig. 11(c), where V_{di} (i=1 ∼ 25) denote the 25 parallel varactor diodes on AMC plane, R is the current limiting resistor.

In this measurement, the DC power supply has been tuned smoothly in the range of 0 – 12 V with the resolution of 0.01 V. By adjusting the DC power supply, the different bias voltages were set, then the reflection coefficients for the active AMC-based antenna were tested. The measured magnitudes of the antenna's S_{11} are shown in Figs. 12(c) and 12(d). It is observed that, when $H = 2$ mm, the AMC-based antenna's operation frequency spans from 1.73 to 1.97 GHz along with the reversely biased voltage, V_r, changing from 0 to 12 V. The minimum return loss is –12.4 dB occurred at about 1.85 GHz with $V_r = 5$ V.

Comparing the results in Fig. 12(c) to those displayed in Fig. 7(c), it is found that, the operation frequency of the proposed active AMC-based antenna has been effectively steered by adjusting the reversely biased voltage on the varactor diodes. Its frequency-tuning capability agrees well with the simulated one realized by using the different lumped capacitors. Due to the inevitable losses introduced by the varactor diodes with parasitic effects and internal resistance [6], the measured magnitudes of S_{11} of the active AMC-based antenna are higher than those simulated results.

Figs. 13(a)-(c) show the measured co-polarization radiation patterns for the antenna at 1.8 GHz with and without using the AMC plane. For the dipole antenna without AMC, its co-polarized radiation pattern exhibits the typical omnidirectional property in H-plane, as seen in Fig. 13(a), with the gain of about 2.21 dBi. When the proposed CFRN-AMC loaded with 1.2 pF capacitors is employed as the reflector

TABLE 2. Comparisons of the proposed active CFRN-AMC-based antenna and the published literatures.

Ref.	AMC metal pattern	Size of AMC unit cell (mm × mm)	Type of AMC	Number of devices for AMC unit cell	Frequency bands of antenna (GHz)	Tunability range	Separation distance between antenna and AMC	Max. gain (dBi)	Reconfigurable antenna
[4]	Square patch with slots	14.7 × 14.7 (0.11λ×0.11λ)	passive	–	1.7-2.7	–	6.2 mm (0.04λ)	7.3	No
[24]	Double-square patch	25 × 25 (0.12λ×0.12λ)	passive	–	1.38, 1.57	–	3 mm (0.014λ)	2	No
[25]	Double-circle patch	26 × 26 (0.21λ×0.21λ)	passive	–	2.4, 5.2	–	3 mm (0.024λ)	7.3	No
[26]	Cross-loaded loops	25 × 25 (0.42λ×0.42λ)	passive	–	5	–	5 mm (0.083λ)	6.36	No
[27]	Square patch	33 × 33 (0.16λ×0.16λ)	passive	–	1.19-2.37	–	15 mm (0.072λ)	6	No
[1]	Square patch	38 × 38 (0.04λ×0.04λ)	active	4 or 8 varactors	–	–	–	–	–
[2]	Square patch	21.4 × 21.4 (0.18λ×0.18λ)	active	1 varactor	2.26-2.75	1.22	3 mm (0.025λ)	5	Yes
[6]	Square patch	18 × 18 (0.13λ×0.13λ)	active	4 varactors	1.75-2.73	1.56	5.5mm (0.041λ)	6.6	Yes
[22]	Circle ring	23 × 23 (0.12λ×0.12λ)	active	2 varactors and 2 resistors	1.15-1.6	1.39	5 mm (0.027λ)	3.7	Yes
This work	**CFRN**	**25 × 25 (0.15λ×0.15λ)**	**active**	**1 varactor**	**1.51-2.12**	**1.40**	**2 mm (0.012λ)**	**5.37**	**Yes**

* λ is the wavelength in free space at the center frequency for the corresponding wideband and reconfigurable antenna, or at the center frequency of the lower band for a dual-band antenna.

for the antenna, no matter that H is set as 2 or 10 mm, the maximum radiation of the antenna remains in the vertical direction above the AMC plane, due to the effect of the in-phase reflection of the AMC. This significantly enhances the antenna's directivity in H-plane, and the maximum gain reaches 5.37 and 6.18 dBi, respectively, as depicted in Figs. 13(b) and 13(c).

It is also found that the E-plane co-polarized radiation pattern of the dipole antenna seems to be a little affected by the AMC, and it still keeps an approximate 8-shaped pattern except that its radiation gain has been increased. The different influences of the AMC reflector on E-plane and H-plane co-polarized radiation patterns of the antenna can be attributed to the fact that the AMC plane is parallel to the electric field of the dipole antenna. Because of the effect of the in-phase reflection of the AMC reflector, the circular doughnut-shaped radiation pattern will stack upward to form a hemispherical shape, and its cross-section still maintains an 8-shaped pattern.

The cross-polarization radiated fields for the antennas without and with the AMC ground are displayed in Figs. 13(d)-(f). It is observed that, both the cross-polarized H-plane and E-plane radiation patterns of the dipole antenna are little affected by the AMC ground, while their radiation gains have been increased when the AMC ground exists.

Table 2 summarizes the characteristics of the proposed active CFRN-AMC-based antenna and the related published literatures with the different AMC metal structures. It is noticed that although the single-band, dual-band or wideband passive AMC-based antennas sometimes exhibit high gain [4], [25]–[27], they cannot be reconfigured and generally require a high profile structure.

The proposed frequency-reconfigurable CFRN-AMC-based antenna holds the minimum distance between the antenna and the AMC plane. Its tunability range specified as the ratio of the upper to lower frequencies, reaches about 1.40, which is better than 1.22 presented in [2] and 1.39 in [22].

In addition, in comparison to other active AMC or AMC-based antennas [1], [2], [6], [27], this CFRN-AMC-backed antenna achieves relatively high gain and uses only one varactor diode in the AMC unit cell. The reduction of the number of varactor diodes will greatly improve the stability of the active AMC-based antenna system and reduce the production cost.

V. CONCLUSION

In this paper, a novel active CFRN-AMC loaded with varactor diodes is presented, whose equivalent circuits have been developed and analyzed. It is found that the varactor capacitance cannot only improve to control the operation frequency band of the AMC easily but also lower its resonant frequency with smaller AMC's dimensions. To realize the frequency-reconfigurable antenna, a triangle-shaped dipole antenna is placed over the active CFRN-AMC plane. The simulation and measurement results show that the presented CFRN-AMC-based antenna exhibits the characteristics of frequency-reconfiguration, high gain enhancement, as well as very low profile. The separation distance between the dipole antenna and the AMC plane is only 2 mm, or 0.012λ at 1.8 GHz.

REFERENCES

[1] T. Li, H. Yang, Q. Li, X. Zhu, X. Cao, J. Gao, and Z. Wu, "Dual-polarised and ultra-thin broadband AAMCs for both p and l bands applications," *IET Microw., Antennas Propag.*, vol. 13, no. 2, pp. 185–189, Feb. 2019.

[2] F. Costa, A. Monorchio, S. Talarico, and F. M. Valeri, "An active high-impedance surface for low-profile tunable and steerable antennas," *IEEE Antennas Wireless Propag. Lett.*, vol. 7, pp. 676–680, 2008.

[3] H. Sun and S. Sun, "A novel reconfigurable feeding network for quad-polarization-agile antenna design," *IEEE Trans. Antennas Propag.*, vol. 64, no. 1, pp. 311–316, Jan. 2016.

[4] M. Li, Q. L. Li, B. Wang, C. F. Zhou, and S. W. Cheung, "A low-profile dual-polarized dipole antenna using wideband AMC reflector," *IEEE Trans. Antennas Propag.*, vol. 66, no. 5, pp. 2610–2615, May 2018.

[5] F. Wu and K. M. Luk, "Single-port reconfigurable magneto-electric dipole antenna with quad-polarization diversity," *IEEE Trans. Antennas Propag.*, vol. 65, no. 5, pp. 2289–2296, May 2017.

[6] D. Chen, W. Yang, W. Che, Q. Xue, and L. Gu, "Polarization-reconfigurable and frequency-tunable dipole antenna using active AMC structures," *IEEE Access*, vol. 7, pp. 77792–77803, Jun. 2019.

[7] S. V. Hum, M. Okoniewski, and R. J. Davies, "Realizing an electronically tunable reflectarray using varactor diode-tuned elements," *IEEE Microw. Wireless Compon. Lett.*, vol. 15, no. 6, pp. 422–424, Jun. 2005.

[8] K. K. Tsang and R. J. Langley, "Annular ring microstrip antennas on biased ferrite substrates," *Electron. Lett.*, vol. 30, no. 16, pp. 1257–1258, Aug. 1994.

[9] T. Li, H. Zhai, X. Wang, L. Li, and C. Liang, "Frequency-reconfigurable bow-tie antenna for Bluetooth, WiMAX, and WLAN applications," *IEEE Antennas Wireless Propag. Lett.*, vol. 14, pp. 171–174, 2015.

[10] M. Borhani, P. Rezaei, and A. Valizade, "Design of a reconfigurable miniaturized microstrip antenna for switchable multiband systems," *IEEE Antennas Wireless Propag. Lett.*, vol. 15, pp. 822–825, 2016.

[11] A. Boukarkar, X. Q. Lin, J. W. Yu, P. Mei, Y. Jiang, and Y. Q. Yu, "A highly integrated independently tunable triple-band patch antenna," *IEEE Antennas Wireless Propag. Lett.*, vol. 16, pp. 2216–2219, 2017.

[12] Y. Liu, P. Liu, Z. Meng, L. Wang, and Y. Li, "A planar printed nona-band loop-monopole reconfigurable antenna for mobile handsets," *IEEE Antennas Wireless Propag. Lett.*, vol. 17, no. 8, pp. 1575–1579, Aug. 2018.

[13] H.-W. Deng, T. Xu, and F. Liu, "Broadband pattern-reconfigurable filtering microstrip antenna with quasi-Yagi structure," *IEEE Antennas Wireless Propag. Lett.*, vol. 17, no. 7, pp. 1127–1131, Jul. 2018.

[14] R. K. Mishra, S. S. Pattnaik, and N. Das, "Tuning of microstrip antenna on ferrite substrate," *IEEE Trans. Antennas Propag.*, vol. 41, no. 2, pp. 230–233, Feb. 1993.

[15] K. A. Jose, V. K. Varadan, and V. V. Varadan, "Experimental investigations on electronically tunable microstrip antennas," *Microw. Opt. Technol. Lett.*, vol. 20, no. 3, pp. 166–169, Feb. 1999.

[16] J. Wu, S. Yang, Y. Chen, S. Qu, and Z. Nie, "A low profile dual-polarized wideband omnidirectional antenna based on AMC reflector," *IEEE Trans. Antennas Propag.*, vol. 65, no. 1, pp. 368–374, Jan. 2017.

[17] A. Mersani, L. Osman, and J.-M. Ribero, "Performance of dual-band AMC antenna for wireless local area network applications," *IET Microw., Antennas Propag.*, vol. 12, no. 6, pp. 872–878, May 2018.

[18] K. N. Paracha, S. K. A. Rahim, P. J. Soh, M. R. Kamarudin, K.-G. Tan, Y. C. Lo, and M. T. Islam, "A low profile, dual-band, dual polarized antenna for indoor/outdoor wearable application," *IEEE Access*, vol. 7, pp. 33277–33288, Mar. 2019.

[19] A. Ghosh, T. Mandal, and S. Das, "Design of triple band slot-patch antenna with improved gain using triple band artificial magnetic conductor," *Radio Eng.*, vol. 25, no. 3, pp. 1–7, 2016.

[20] C. Yu, S. Yang, Y. Chen, and D. Zeng, "Radiation enhancement for a triband microstrip antenna using an AMC reflector characterized with three zero-phases in reflection coefficient," *J. Electromagn. Waves Appl.*, vol. 33, no. 14, pp. 1846–1859, Jul. 2019.

[21] B. Sanz-Izquierdo and E. A. Parker, "Dual polarized reconfigurable frequency selective surfaces," *IEEE Trans. Antennas Propag.*, vol. 62, no. 2, pp. 764–771, Feb. 2014.

[22] B. Sanz-Izquierdo, B. Liang, E. A. Parker, and J. C. Batchelor, "An application of active frequency selective surface to reconfigurable antenna technology," in *Proc. Act. Passive RF Devices Seminar*, London, U.K., Feb. 2016, pp. 1–5.

[23] F. Costa, A. Monorchio, and G. P. Vastante, "Tunable high-impedance surface with a reduced number of varactors," *IEEE Antennas Wireless Propag. Lett.*, vol. 10, pp. 11–13, Jun. 2011.

[24] J. Lin, Z. Qian, W. Cao, S. Shi, Q. Wang, and W. Zhong, "A low-profile dual-band dual-mode and dual-polarized antenna based on AMC," *IEEE Antennas Wireless Propag. Lett.*, vol. 16, pp. 2473–2476, 2017.

[25] H. Zhai, K. Zhang, S. Yang, and D. Feng, "A low-profile dual-band dual-polarized antenna with an AMC surface for WLAN applications," *IEEE Antennas Wireless Propag. Lett.*, vol. 16, pp. 2692–2695, 2017.

[26] M. M. Mostafa, T. M. Abuelfadl, and A. M. E. Safwat, "AMC loaded folded dipole with heart-shaped radiation pattern," *Electron. Lett.*, vol. 54, no. 18, pp. 1061–1062, Sep. 2018.

[27] D. Feng, H. Zhai, L. Xi, S. Yang, K. Zhang, and D. Yang, "A broadband low-profile circular-polarized antenna on an AMC reflector," *IEEE Antennas Wireless Propag. Lett.*, vol. 16, pp. 2840–2843, 2017.

[28] Y. F. Cao and X. Y. Zhang, "A wideband beam-steerable slot antenna using artificial magnetic conductors with simple structure," *IEEE Trans. Antennas Propag.*, vol. 66, no. 4, pp. 1685–1694, Apr. 2018.

[29] J. Li, H. Huo, J. Chen, S. Zhu, H. Shi, and A. Zhang, "Miniaturised artificial magnetic conductor and its application in unidirectional circularly polarised slot antenna design," *IET Microw., Antennas Propag.*, vol. 12, no. 12, pp. 1885–1889, Oct. 2018.

[30] X. Li, Y.-C. Jiao, and L. Zhang, "Wideband low-profile CPW-fed slot-loop antenna using an artificial magnetic conductor," *Electron. Lett.*, vol. 54, no. 11, pp. 673–674, May 2018.

[31] C. Ning, W.-Y. Yin, J. Jin, K. Yang, H. Xie, D. W. Wang, Y. Liao, L. D. Wang, H. S. Chen, and E. P. Li, "Notice of retraction: A novel electromagnetic bandgap power plane etched with multiring CSRRs for suppressing simultaneous switching noise," *IEEE Trans. Electromagn. Compat.*, vol. 60, no. 3, pp. 733–737, Jun. 2018.

[32] O. Luukkonen, C. R. Simovski, A. V. Räisänen, and S. A. Tretyakov, "An efficient and simple analytical model for analysis of propagation properties in impedance waveguides," *IEEE Trans. Microw. Theory Techn.*, vol. 56, no. 7, pp. 1624–1632, Jul. 2008.

[33] L.-F. Shi, K.-J. Li, H.-Q. Hu, and S. Chen, "Novel L-EBG embedded structure for the suppression of SSN," *IEEE Trans. Electromagn. Compat.*, vol. 58, no. 1, pp. 241–248, Feb. 2016.

[34] S. Shi, P. Yang, L. Zhou, and W. Chen, "Wideband planar dipole based on dual-layer artificial magnetic conductor," *J. Eng.*, vol. 2019, no. 19, pp. 6180–6183, Oct. 2019.

[35] J. Zhang, X. Q. Lin, L. Y. Nie, J. W. Yu, and Y. Fan, "Wideband dual-polarization patch antenna array with parallel strip line Balun feeding," *IEEE Antennas Wireless Propag. Lett.*, vol. 15, pp. 1499–1501, 2016.

[36] M. Li, Q. Li, B. Wang, C. Zhou, and S. Cheung, "A miniaturized dual-band base station array antenna using band notch dipole antenna elements and AMC reflectors," *IEEE Trans. Antennas Propag.*, vol. 66, no. 6, pp. 3189–3194, Jun. 2018.

[37] M. Li, R. Wang, J. M. Yasir, and L. Jiang, "A miniaturized dual-band dual-polarized band-notched slot antenna array with high isolation for base station applications," *IEEE Trans. Antennas Propag.*, vol. 68, no. 2, pp. 795–804, Feb. 2020.

SHUHUI YANG (Member, IEEE) received the B.Sc. degree from Zhejiang University, in 1994, the M.Sc. degree from the Beijing Broadcasting Institute, in 1997, and the Ph.D. degree from the Institute of Microelectronics, Chinese Academy of Sciences, in 2003.

From 2003 to 2015, he was with the Beijing Information and Science Technology University as a Professor. In 2015, he joined the Communication University of China as a Professor and the Chairman of the Department of Communication Engineering. In 2008, he was a Visiting Scholar and an Adjunct Associate Professor with the University of South Carolina (USC), Columbia, SC, USA. From 2013 to 2014, he was a Visiting Professor with USC. He has published more than 90 articles in technical journals and conferences and coauthored over five books. His current research interests include AMC-based antennas, MIMO antennas, filters, and metamaterials. He is the Senior Member of the Chinese Institute of Electronics (CIE).

YINCHAO CHEN (Senior Member, IEEE) received the Ph.D. degree in electrical engineering from the University of South Carolina.

Since then, he has been worked with the University of Illinois at Urbana-Champaign (UIUC), The Hong Kong Polytechnic University (HKPU), and the University of South Carolina (USC), respectively. He is one of coauthors or editors for three academic books and ten book chapters in electrical engineering, and has published more than 200 academic articles in international journals and conference proceedings. His current research interests include signal integrity for high speed circuits, RF and integrated microwave circuits, and integrated microstrip antennas.

CHENYIN YU received the B.S. degree from the Communication University of China (CUC), in 2017, where she is currently pursuing the master's degree with the Department of Communication Engineering. Her current research interests include MIMO antennas and metasurfaces.

YAJIE GONG is currently pursuing the B.S. degree with the Department of Communication Engineering, Communication University of China (CUC). Her current research interests include active AMCs and AMC-based antennas.

FANGLU TONG is currently pursuing the B.S. degree with the Department of Communication Engineering, Communication University of China (CUC). Her current research interests include AMC-based antennas and metasurfaces.